

## Buckling analysis of perforated square plates with different oriented various shaped polygon holes

*Farklı açılardaki çeşitli çokgen delikli kare plakların burkulma analizi*

Mustafa Halûk SARAÇOĞLU<sup>1</sup> , Fethullah USLU<sup>2</sup> , Uğur ALBAYRAK<sup>3</sup> 

<sup>1</sup>Kütahya Dumlupınar Üniversitesi, Mühendislik Fakültesi, İnşaat Mühendisliği Bölümü, 43100, Kütahya

<sup>2</sup>Eskişehir Osmangazi Üniversitesi, Mühendislik-Mimarlık Fakültesi, İnşaat Mühendisliği Bölümü, 26480, Eskişehir

• Received: 20.07.2023

• Accepted: 03.11.2023

### Abstract

Buckling of the plates is of great importance in design of structures. If the plate has a hole because of necessity, hole area and shape also affect the critical buckling loads. In this study, buckling analyses of perforated simply supported square plates with various perforation patterns and different loading types were investigated. Three different perforation patterns as circular, hexagonal and square with different orientations were considered. In order to investigate the slenderness ratio effect, samples were calculated with three different ratio values of 100, 20 and 10. The samples were loaded with four different in-plane loads to examine the effect of loading type. Analyses were performed by using a general purpose finite element program and critical buckling loads were determined depending on the orientation angles for square plate models with different hole perforations. The critical buckling load is independent from the orientation angle for circular perforated plates but depends on for hexagonal and square hole perforations. For these plates buckling analyses were performed for different orientation angles of 0 degrees to 90 degrees. The results show that the calculated critical buckling loads did not remain the same although the hole areas were the same.

**Keywords:** Buckling analysis, Hexagonal hole, Orientation angle, Perforated plates

### Öz

Plakların burkulması, yapıların tasarımında büyük önem taşımaktadır. Plakta zorunlu olarak bir delik olması gerekiyorsa, delik alanı ve şekli de kritik burkulma yüklerini etkileyecektir. Bu çalışmada, çeşitli delik şekillerine ve farklı yükleme tiplerine sahip delikli basit mesnetli kare plakaların burkulma analizleri incelenmiştir. Farklı dönme açılına sahip dairesel, altıgen ve kare olmak üzere üç farklı delik şekli modeli dikkate alınmıştır. Narinlik oranı etkisini araştırmak için ise örnekler 100, 20 ve 10 olmak üzere üç farklı narinlik oranı değeri ile hesaplanmıştır. Yükleme tipinin etkisini incelemek için numuneler dört farklı düzlem içi yük ile yüklenmiştir. Analizler genel amaçlı bir sonlu elemanlar programı kullanılarak gerçekleştirilmiş ve farklı çokgen deliklere sahip kare plak modelleri için dönme açılına bağlı olarak kritik burkulma yükleri belirlenmiştir. Kritik burkulma yükü, dairesel delikli plakalar için dönme açısından bağımsızdır, ancak altıgen ve kare delikli delikler için bağımlı olacaktır. Bu plaklar için 0 dereceden 90 dereceye kadar farklı dönme açıları için burkulma analizleri yapılmıştır. Sonuçlar, delik alanları aynı olmasına rağmen hesaplanan kritik burkulma yüklerinin aynı kalmadığını göstermektedir.

**Anahtar kelimeler:** Burkulma analizi, Altıgen delik, Dönme açısı, Delikli plak

\*Mustafa Halûk SARAÇOĞLU; mhaluk.saracoglu@dpu.edu.tr

## 1. Introduction

In structural design, buckling analyses have an important aspect. Holes of different sizes and different geometries can be constructed in the plates in case of necessity. These holes in the perforated plate change the stiffness of the plate. This change will affect the stress distribution and also the buckling failure mode of the plate.

Many studies on perforated plates have been made and published. Timoshenko and Woinowsky-Krieger (Timoshenko & Woinowsky-Krieger, 1959) presented the differential equation and solution for axially loaded plate in their work, which is used as the basic book in all plate studies. Brown et al (Brown et al., 1987) investigated the stability of plates with rectangular holes. In their study different loadings and different boundary conditions considered. Albayrak and Saraçoğlu (Albayrak & Saraçoğlu, 2018) studied about perforated thin plates with various hole patterns which are simply supported on all its boundaries. They performed the plates on various models systematically by number, diameter and location of holes. At the end of the study, they find out the optimum hole pattern for circular perforated plates by using APDL codes based on Finite Element Method. Chow and Narayanan (Chow & Narayanan, 1984) studied the elastic buckling behavior of simply and fixed supported square plates containing holes. In their study, the position and size of the square and circular holes on the plate were taken as parameters and experimental results were compared with the results obtained by the computational methods. Guo and Yao (Guo & Yao, 2021) studied buckling behavior of perforated thin plates. They presented the buckling coefficients of perforated plates with rectangular or circular holes by using the extensive parametric study results obtained by finite element method. Saraçoğlu et al (Saraçoğlu et al., 2021) employed a computational model for perforated thin steel square plates bearing uniformly distributed loads that have simply and fixed supported boundary conditions in their study. Dehadray et al (Dehadray et al., 2021) investigated the critical buckling loads for square aluminum and steel square plates with rectangular cut-outs for simply supported boundary conditions in their study. The results are calculated for different parameters as thickness, aspect ratio and variation in orientation of cut-out. Silveira et al (Silveira et al., 2021) applied the constructal design method for investigating the numerical analysis of biaxial buckling of perforated rectangular steel plates. Jayabalan et al (Jayabalan et al., 2022) used different techniques for estimating the buckling coefficients of steel plates with central cutouts. They compared the results obtained by using various techniques from the literature as Evolutionary Polynomial Regression, Artificial Neural Network and Gene Expression Programming. Qablan (Al Qablan, 2022) created formulations for thermal and axially in-plane loaded perforated plates with different boundary conditions in his study. Kharchenko (Kharchenko et al., 2022) et al determined the durability of sieves with different types of holes in their study. They used different hole shapes like triangular and analyzed the problems by using the finite element method based software and experimental data. Karakaya (Karakaya, 2022) investigate the mechanical behavior of linear and staggered arranged circle, triangle, square, hexagon, and ellipse perforated stainless steel and aluminum sheets under tensile loading by finite element analysis in his study. Uslu et al (Uslu et al., 2022) investigate the critical buckling loads of simply supported uniaxially loaded square thin plates with central square and circular holes in terms of some parameters. Fu and Wang (Fu & Wang, 2022) developed a new semi-analytical modelling technique to calculate the critical buckling load of perforated plates with opposite free edges. Perforated plates with central circular holes were discussed as case studies and the results were compared with those obtained from finite element method. Al Qablan et al (Al Qablan et al., 2022) developed a closed-form semi-empirical formula for calculating a critical buckling load for perforated composite panels. They interested in simply and clamped supported composite circular perforated plates subjected to uniaxial and biaxial loadings in their study. Baumgardt et al (Baumgardt et al., 2023) developed a model in their study and simulated the mechanical behavior of plates under uniaxial and biaxial in-plane loadings. They also examined the perforated plates with different hole geometries such as circle, square, and rectangle perforations.

Since the geometry of the circle, which we can define as a polygon consisting of an infinite number of edges, is symmetrical, it will give the same geometry no matter what angle it rotates around its center point. This case will not apply to polygons with a different number of edges. Especially in perforated plates that are subjected to in-plane forces such as uniaxial or biaxial buckling loads, the internal forces occurring in the structural element will differ depending on the orientation angle around the center of the polygon hole. In this study effects of the orientation angle of different polygon holes as square and hexagon on critical buckling loads for square plates are investigated. Though there have also been numerous studies on analyses of plates with holes, few are seen in open literature on plates with different hole shapes from circular, rectangular and square.

Different from the usual shapes, an investigation of hexagonal perforated plates was also carried out in this study.

## 2. Material and method

Thin plates can be subjected to axial compressive loads acting on the plate midplane. Such loads can cause buckling of the plate under certain conditions. In practical applications buckling of the plates is of great importance. Plate thickness is a parameter that directly affects the critical buckling load. If the plate thickness is low, the critical buckling load will be less depending on the thickness. The buckling analysis of plates has very important in the analysis of structures.

When the axial compressive loads acting on the plate exceed the critical buckling value, very large lateral deflections will occur in the plate. Because of this loading, very large bending stresses will occur and eventually, the plate will not be able to carry the load and will collapse.

As the plate equilibrium goes from a stable configuration to unstable configuration, it will pass through the neutral state of equilibrium, which is a boundary state. In mathematical expressions of the plate buckling problems, the neutral state of equilibrium can be obtained from the deformations. The critical buckling load that can be applied to the plate can be defined as the smallest possible load that causes it to pass from the neutral state of equilibrium to the unstable state. The purpose of buckling analyses in plates is to determine these critical buckling loads.

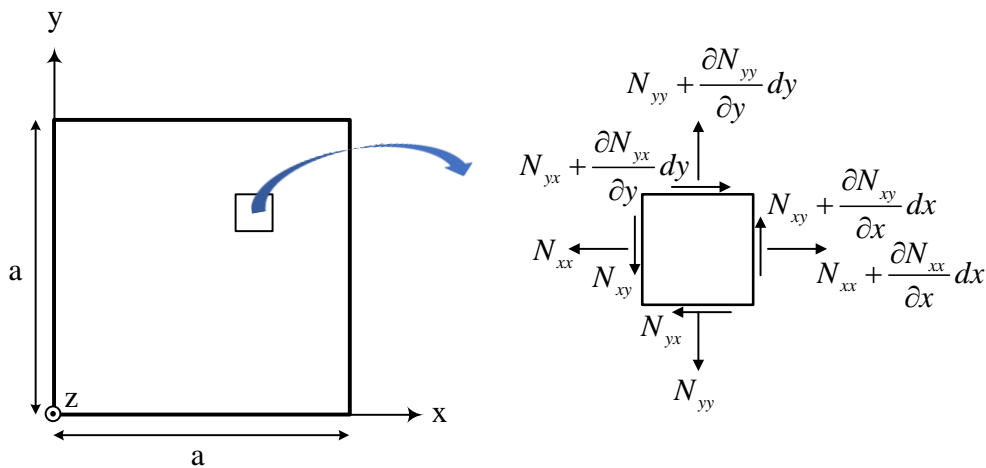


**Figure 1.** Stress resultants of a differential element in a plate

The corresponding in-plane stress resultants  $N_{xx}$ ,  $N_{yy}$  and  $N_{xy}$  can be found from the solution of the plane stress problem for a given plate geometry and in-plane external loading in the initial equilibrium state of a plate subjected to external edge loads acting on the midplane of the plate (Figure 1). When the vertical equilibrium equation in z direction is written in a differential element by using these expressions, the governing differential equation in the linear buckling analysis of the plate is obtained as in Equation (1).

$$\frac{\partial^4 w}{\partial x^4} + 2 \frac{\partial^4 w}{\partial x^2 \partial y^2} + \frac{\partial^4 w}{\partial y^4} = \frac{1}{D} \left( N_{xx} \frac{\partial^2 w}{\partial x^2} + 2N_{xy} \frac{\partial^2 w}{\partial x \partial y} + N_{yy} \frac{\partial^2 w}{\partial y^2} \right) \quad (1)$$

In this expression,  $N_{xx}$ ,  $N_{yy}$  and  $N_{xy}$  are in-plane stress resultants.  $D$  defines the bending stiffness of the isotropic plate which has  $h$  thickness,  $E$  modulus of elasticity and  $\nu$  Poisson's ratio as in Equation (2).

$$D = \frac{E h^3}{12(1-\nu^2)} \quad (2)$$

To calculate the critical buckling load, this homogeneous partial differential equation needs to be solved with appropriate boundary conditions. Simply support boundary conditions for a square plate can be defined as in Equation (3).

$$w = 0 \Big|_{x=0,a} \quad \frac{\partial^2 w}{\partial x^2} = 0 \Big|_{x=0,a} \quad w = 0 \Big|_{y=0,a} \quad \frac{\partial^2 w}{\partial y^2} = 0 \Big|_{y=0,a} \quad (3)$$

If the buckling load is uniaxial, the governing differential equation becomes as in Equation (4).

$$D \left( \frac{\partial^4 w}{\partial x^4} + 2 \frac{\partial^4 w}{\partial x^2 \partial y^2} + \frac{\partial^4 w}{\partial y^4} \right) - \left( N_{xx} \frac{\partial^2 w}{\partial x^2} \right) = 0 \quad (4)$$

This constant coefficient linear partial differential equation can be solved by converting it into a two-harmonic equation. The solution of this expression that satisfies the simple support boundary conditions can be defined by the expression of infinite series as in Equation (5).

$$\sum_{m=1}^{\infty} \sum_{n=1}^{\infty} \left[ D \pi^4 \left( \frac{m^2}{a^2} + \frac{n^2}{b^2} \right) - q_x \pi^2 \frac{m^2}{a^2} \right] w_{mn} \sin \frac{m\pi x}{a} \sin \frac{n\pi y}{b} = 0 \quad (5)$$

One possible solution of this expression can be obtained by setting the quantity in square brackets to zero as in Equation (6).

$$\left[ D \pi^4 \left( \frac{m^2}{a^2} + \frac{n^2}{b^2} \right) - q_x \pi^2 \frac{m^2}{a^2} \right] = 0 \quad (6)$$

From this equation load  $q_x$  can be calculated as in Equation (7).

$$q_x = \frac{\pi^2 D}{b^2} \left( \frac{mb}{a} + \frac{n^2 a}{mb^2} \right)^2 \quad (7)$$

This expression gives all values of  $q_x$  corresponding to  $m = 1, 2, 3, \dots$  and  $n = 1, 2, 3, \dots$  as possible forms of the deflected surface of the plate. The smallest value of these values is the critical one and can be obtained for  $n = 1$  as in Equation (8).

$$N_{xx} = \frac{\pi^2 D}{b^2} \left( \frac{mb}{a} + \frac{a}{mb^2} \right)^2 \quad (8)$$

This value depends only on the aspect ratio of the plate for a known  $m$  value. From this equation the elastic critical stress of a simply supported square plates can be calculated as in Equations (9) and (10) (Bryan, 1891; Guo & Yao, 2021).

$$\sigma_{cr} = \frac{\pi^2 D}{hb^2} \left( \frac{mb}{a} + \frac{a}{mb} \right)^2 \quad (9)$$

$$\sigma_{cr} = k \frac{\pi^2 E}{12(1-\nu^2)(a/h)^2} = k \frac{\pi^2 D}{a^2 h} \quad (10)$$

In this equation  $k$  is the plate buckling coefficient. If  $D$  is the plate flexural rigidity (Timoshenko, & Woinowsky-Krieger, 1959), plate buckling coefficient can be expressed as in Equation (11).

$$k = \sigma_{cr} \frac{a^2 h}{\pi^2 D} \quad \text{or} \quad k = \frac{a^2}{\pi^2 D} N_{cr} \quad (11)$$

These problems solved by using the finite element package program ANSYS (Swanson Analysis System Inc., 2005).

In this computational study, SHELL 181 element, as shown in Figure 2, has been selected from the finite element software program library. This element has 4 nodes. Each node has 6 degrees of freedom. These freedoms are translations and rotations in 3 axes (x-y-z)

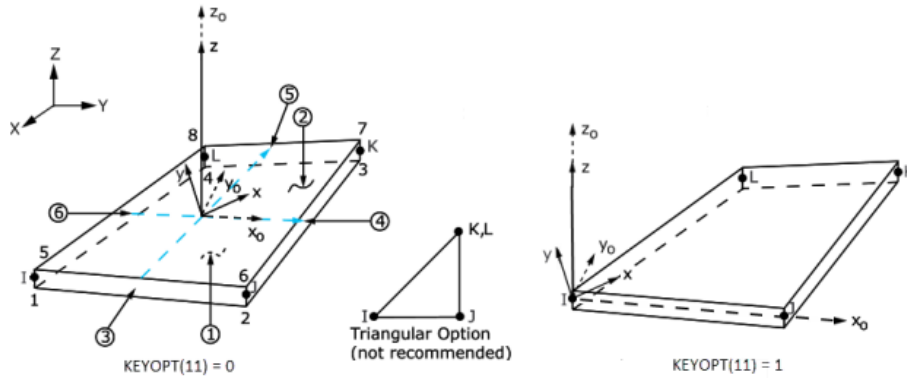


Figure 2. SHELL181 finite element of ANSYS program (Swanson Analysis System Inc., 2005)

In computational mechanics mesh convergence effects, the accuracy of problem results. For determining the correct finite element mesh density different finite element frequencies created for the analyzed plate models and different results are obtained. From the mesh convergence study, it was observed that the difference between the results was negligible if the mesh spacing was below 10 mm. The mesh spacing was chosen as 10 mm so that the calculation results do not deviate from the exact value and the analysis time does not prolong too much.

### 2.1. Verification of models

For the purpose of verification of the models, the critical buckling loads of the square hole perforated plate taken from the literature were analyzed by using finite element software for uniaxial and biaxial cases. For this purpose, the results obtained by finite element method are compared to those results given by literature (Chow & Narayanan, 1984). The buckling coefficient is calculated as in the derived equation before.

As an example, the contour plots of the total deformation of perforated square plates with square holes with a/h=100 slenderness ratios under uniaxial and biaxial loadings are shown in Figure 3.

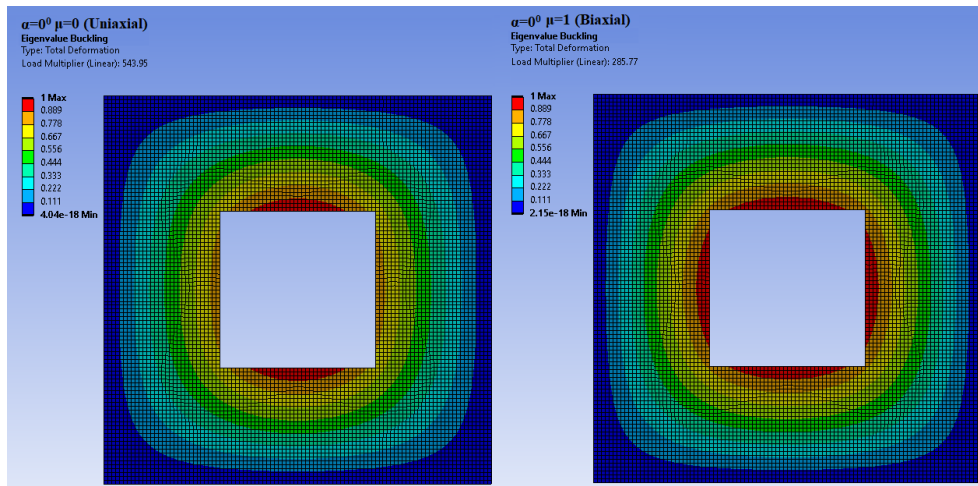


Figure 3. Contour plots of total deformations for square perforated plates (a/h=100)

The buckling coefficients obtained by the finite element for the simply supported square plates with square holes with different thickness and the corresponding values obtained from Chow and Narayanan (Chow & Narayanan, 1984) are listed in Table 1. Length of square steel plate is taken as 1000 mm. A square hole is perforated, in the middle of the square plate, and the one length of the square hole was taken as 500mm which is half of the square plate length.

**Table 1.** Comparison of square hole perforated plates with reference.

Loading	a/h	$N_{cr}^{FE}$ (N/mm)	$k^{FE}$	$N_{cr}^{(Cho.&Nar.)}$ (N/mm)	$k^{(Cho.&Nar.)}$	$k^{Dif. \%}$	$N_{cr}^{Dif. \%}$
Uniaxial	100	543.95	3.01	547.45	3.03	-0.64	-0.64
	20	65825.56	2.91	68431.31	3.03	-3.81	-3.81
	10	495490.38	2.74	547450.58	3.03	-9.49	-9.49
Biaxial	100	285.77	1.58	283.08	1.57	0.95	0.95
	20	34970.74	1.55	35385.01	1.57	-1.17	-1.17
	10	268876.74	1.49	283080.09	1.57	-5.02	-5.02

Difference% values are calculated by the  $\left(\frac{FE - Ref}{Ref}\right) \times 100$  formula. It can be seen from the Table 1 that the loads and buckling coefficients obtained from finite element method and numerical results from literature did not differ by more than 9.49%. These comparative results prove that the finite element method models presented in this study are sufficiently accurate. In the reference study, results were obtained for only one plate within the thin plate assumptions. All of the plates with different slenderness ratios considered in this study are within the thin plate assumptions. Therefore, comparisons were made with the same reference values in the table.

### 3. Examples

#### 3.1. Material properties

The example plates were assumed to be made of isotropic structural steel whose material properties are defined as modulus of elasticity (E) is 200000MPa and Poisson's ratio ( $\nu$ ) is 0.3.

#### 3.2. Geometry

Three different hole shape as circular, hexagonal and square are considered. The geometry of the perforations can be of the shape of a circle, a hexagonal or a square polygon which are at the center of the square plate. The geometry of the square plates considered in this study is described in Figure 4 with the length and width of a. In all examples, the open area percentage is the same. The perforated plate with hexagonal holes is taken as a reference. The hole sizes of the other two plates were calculated based on the percentage of open area of the hexagonal perforated plate. In the perforated plate with a hexagonal hole, the length of one side of the hexagonal hole is one quarter of the edge of the plate as 250 mm.

A schematic image of the geometry of the square plates with all three different geometric perforations in the middle of the plates are demonstrated in Figure 4. In this figure, location of the hole, and the edges of the hole can be seen and compared exactly among them. The orientation angle  $\alpha$  is also illustrated in Figure 4. The orientation angle  $\alpha$  can be defined as the angle between the lower edge axis of the plate and the lower edge axis of the hole.

In practice, circular perforated plates are widely used. The geometry of the square plate with the circular perforation in the middle of the plate with diameter  $D_c$  is demonstrated in Figure 4. The critical buckling loads of the plates consisting of different orientation angles of the circular hole in the center of the plate will be the same as expected. So that only one model has been evaluated as shown in Figure 4.

The geometry of the square plate with the hexagonal perforation in the middle of the plate with length of the edge  $D_h$  is demonstrated in Figure 4. By rotating the hexagonal hole in the center of the plate, models were created between the orientation angle of 0 and 30 degrees.

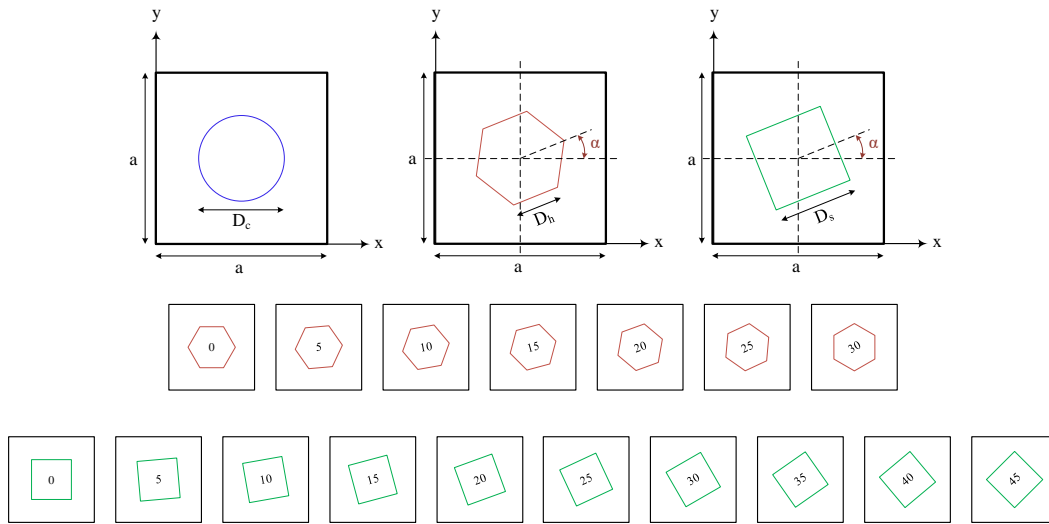


**Figure 4.** Square plate models with different hole perforations and orientations

After the angle of 30 degrees there is a symmetry in the geometry. So that by increasing the orientation angle five by five, seven different models were evaluated as shown in Figure 4.

The geometry of the square plate with the square perforation in the middle of the plate with length of the edge  $D_s$  is demonstrated in Figure 4. By rotating the square hole in the center of the plate, models were created between the orientation angle of 0 and 45 degrees. After the angle of 45 degrees there is a symmetry in the geometry. So that by increasing the orientation angle five by five, ten different models were evaluated as shown in Figure 4.

### 3.3. Loads

Simply supported square plates with a central hole subjected to different in-plane loads are investigated. For this purpose,  $N_{xx}$  load on the perpendicular sides of the square plate to the  $x$ -axis ( $x=0$  and  $x=a$ ) and  $N_{yy}$  load on the sides perpendicular to the  $y$ -axis ( $y=0$  and  $y=a$ ) are defined. There is a relation between the applied  $N_{xx}$  and  $N_{yy}$  buckling loads with the constant  $\mu$  as  $N_{yy} = \mu N_{xx}$ . In example problems different values of  $\mu$  (0, 0.5, 1, 2) is considered. When the value of the coefficient  $\mu$  is 0, problems will be uniaxially loaded, and when the value of the coefficient  $\mu$  is 1, problems will be the bi axially loaded.

For different four values of  $\mu$  as shown in Figure 5 critical buckling loads of perforated simply supported square plates are investigated.

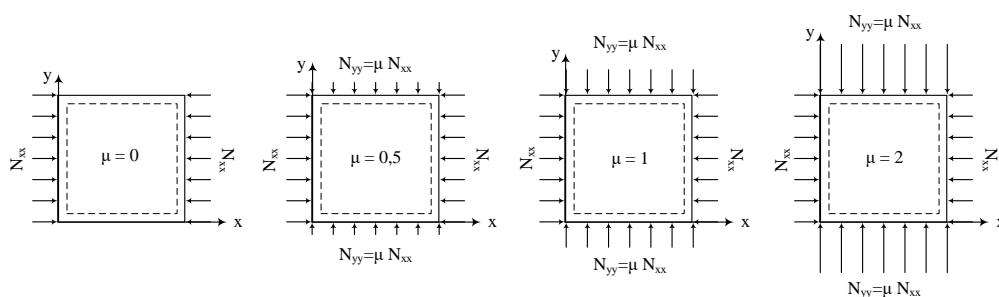


**Figure 5.** Loading types of perforated plates

### 3.4. Boundary conditions

All four edges of the perforated square plates considered in this study are simply supported. Such a boundary condition can be defined by no vertical displacements at the plate edges and zero slopes perpendicular to the plate edges. For this purpose, in the analysis program, on the perpendicular sides of the square plate to the  $x$ -axis ( $x=0$  and  $x=a$ )  $UZ$  and  $ROTX$ , on the sides perpendicular to the  $y$ -axis ( $y=0$  and  $y=a$ )  $UZ$  and  $ROTY$  are

restrained. And also, at the corner points of the plate (0,0) and (a,0) UZ and UY displacements, at the midpoint of the  $y=0$  edge ( $a/2,0$ ) UZ and UX displacements were restrained for the stability of the in-plane loaded plate.

Geometry and boundary conditions for different hole perforations illustrated in Figure 6

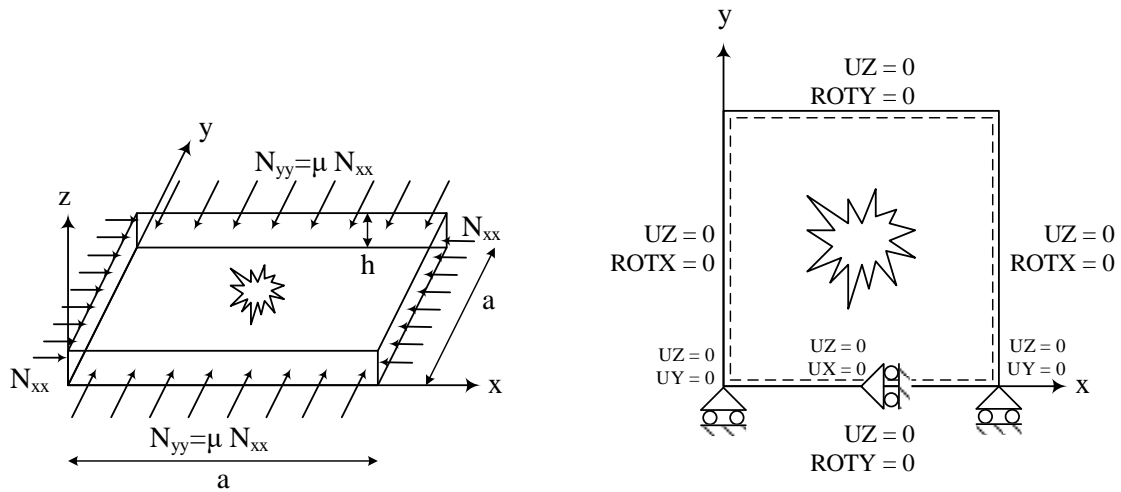


Figure 6. Geometry and boundary conditions of square plate models with different hole perforations

#### 4. Results and discussion

In this section, results on the effect of plate slenderness ratio and hole orientation angle on the critical buckling loads of different shaped perforated simply supported square plates subjected to buckling loads for different biaxial load ratios ( $\mu = N_{yy} / N_{xx}$ ) are presented and discussed. All plate examples conform to Kirchoff-Love thin plate theory assumptions. In this investigation, a general purpose finite element program has used to calculate the critical buckling load of perforated plates.

##### 4.1. Effect of slenderness ratio

The effect of slenderness ratio on the critical buckling loads of different oriented perforated plates are investigated. For this purpose, three different  $h$  thickness (10mm, 50mm, 100mm) considered for constant  $a$  length (1000mm) simply supported square plates.

When the slenderness ratio decreases the critical buckling loads were increases for all types of perforated square plates. The critical buckling loads are the same for circular perforated plates for all orientation angles as expected.

For uniaxial ( $\mu=0$ ) loaded perforated plates critical buckling loads vs orientation angles are plotted in Figure 7 with slenderness ratios 100, 20 and 10 respectively.

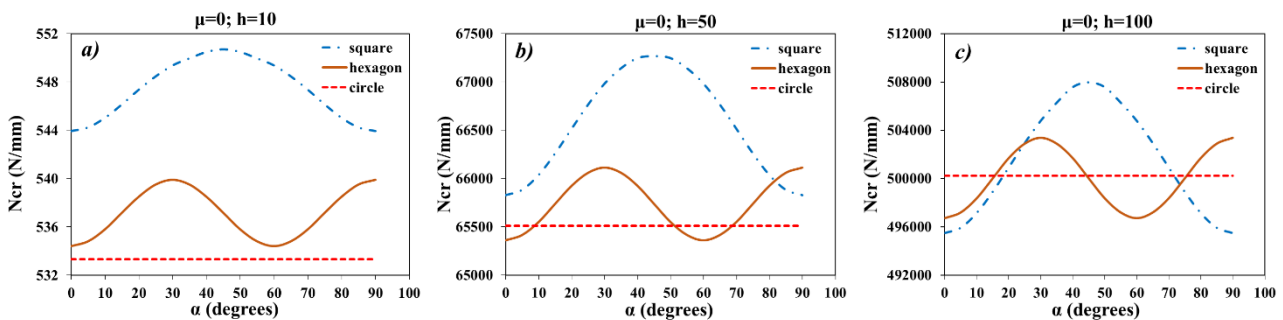


Figure 7. Uniaxial ( $\mu=0$ ) critical buckling loads vs orientation angles for square plate models with different hole perforations (a)  $a/h=100$  (b)  $a/h=20$  (c)  $a/h=10$

In the square perforated plates, it is seen that as the hole orientation increases from 0 to 45 degrees, the critical buckling load also increases regardless of the slenderness ratios. When the orientation angle is 45 degrees in square perforated plates, the critical buckling load is the maximum. Between the 45 to 90 degrees of orientation angle, the critical buckling loads symmetrically decreases, and a frequency occurs between 0 and 90 degrees of orientation angle.

In the hexagonal perforated plates, it is seen that as the hole orientation increases from 0 to 30 degrees, the critical buckling load also increases regardless of the slenderness ratios. When the orientation angle is 30 degrees in hexagonal perforated plates, the critical buckling load is the maximum. Between the 30 to 60 degrees of orientation angle, the critical buckling loads symmetrically decreases, and a frequency occurs between 0 and 60 degrees of orientation angle.

When the slenderness ratio decreases and plates become thicker, the critical buckling loads become closer to each other for the same orientation angles. For the slenderness ratio  $a/h=100$ , the critical buckling loads are ordered from highest to lowest as square, hexagonal and circular perforated plates, respectively. However, when the slenderness ratio decreases this order changes.

For the slenderness ratio  $a/h=20$ , the critical buckling loads for circular perforated plates are higher than the hexagonal perforated plates between 0 to 10 and 50 to 70 degrees of orientation angle. Between 80 to 90 degrees of orientation angle the critical buckling loads for hexagonal perforated plates are higher than the square perforated plates.

For the slenderness ratio  $a/h=10$ , the critical buckling loads for circular perforated plates are higher than the hexagonal and square perforated plates between 0 to 15, higher than the hexagonal perforated plates between 45 to 75 and higher than the square perforated plates between 75 to 90 degrees of orientation angle. Between 0 to 20 and 75 to 90 degrees of orientation angle the critical buckling loads for hexagonal perforated plates are higher than the square perforated plates.

Perforated plates considered in this study were also subjected to compression biaxial loads as uniaxial loads. For biaxial ( $\mu=1$ ) loaded perforated plates critical buckling loads vs orientation angles are plotted in Figure 8 with slenderness ratios 100, 20 and 10 respectively.

In biaxial loading, the critical buckling loads are the same for circular perforated plates for all orientation angles and approximately same for hexagonal perforated plates.

For the slenderness ratio  $a/h=100$ , the critical buckling loads are ordered from highest to lowest as square, hexagonal and circular perforated plates, respectively. However, when the slenderness ratio decreases this order changes.

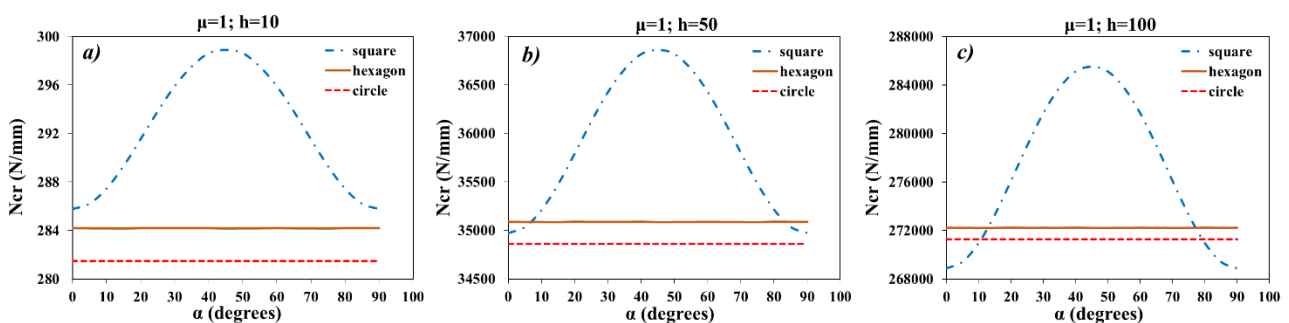


**Figure 8.** Biaxial ( $\mu=1$ ) critical buckling loads vs orientation angles for square plate models with different hole perforations (a)  $a/h=100$  (b)  $a/h=20$  (c)  $a/h=10$

For the slenderness ratio  $a/h=20$ , the critical buckling loads for circular perforated plates are the lowest. Between 0 to 10 and 80 to 90 degrees of orientation angle the critical buckling loads for hexagonal perforated plates are higher than the square perforated plates.

For the slenderness ratio  $a/h=10$ , the critical buckling loads for circular and hexagonal perforated plates are higher than the square perforated plates between 0 to 10 and 80 to 90 degrees of orientation angle. The critical buckling loads for hexagonal perforated plates are higher than the circular perforated plates.

#### 4.2. Effect of loading type

As an example, critical buckling loads vs orientation angles for square plate models with different loading types for slenderness ratio  $a/h=100$  is shown in Figure 9.

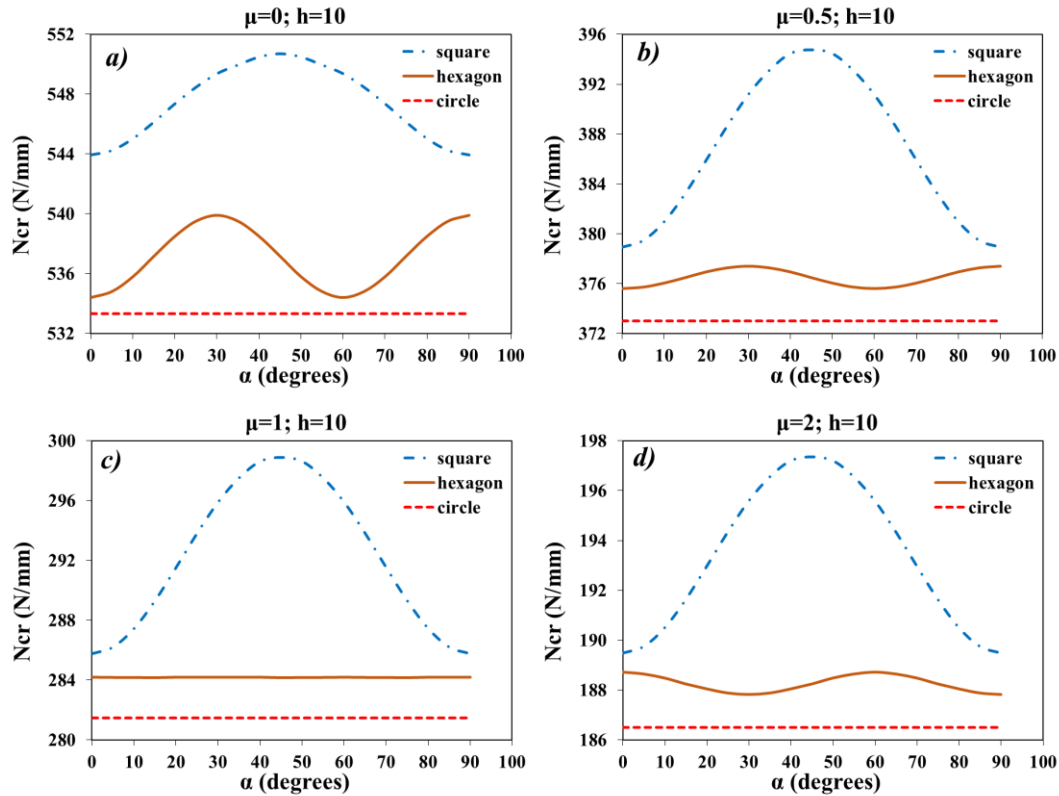


**Figure 9.** Critical buckling loads vs orientation angles for square plate models with different loading types ( $a/h=100$ ) a)  $\mu=0$  b)  $\mu=0.5$  c)  $\mu=1$  d)  $\mu=2$

When the load factor  $\mu$  increases the critical buckling loads decrease. In all cases the critical buckling loads are ordered from highest to lowest as square, hexagonal and circular perforated plates, respectively. The frequency explained before between 0 to 90 degrees of orientation angle can be observed clearly in the critical buckling loads vs orientation angles diagram for square perforated plates.

The frequency between 0 and 60 degrees of orientation angle can be seen for hexagonal perforated plates for load factor  $\mu=0$  and  $\mu=0.5$ . for load factor  $\mu=2$ , in-plane loads in y axis is higher than in x axis. Therefore, the frequency in the diagram takes place inversely.

As a result of analyses, some example drawings shown below. In these drawings uniaxial ( $\mu=0$ ) and biaxial ( $\mu=1$ ) loaded simply supported thin plates have  $a/h=100$  slenderness ratio is considered. For hexagonal perforated plates, four of seven models are selected as an arrangement changed from a horizontal one to a vertical one, whose orientation angles  $\alpha$  are 0, 10, 20, and 30 respectively.

A similar case exists for perforated plates with square holes. For square perforated plates, four of ten models are selected as an arrangement changed from a horizontal one to a vertical one, whose orientation angles  $\alpha$  are 0, 15, 30, and 45 respectively.

The contour plots of total deformations of four of seven different hexagonal perforated plates are given in Figure 10 as an example.

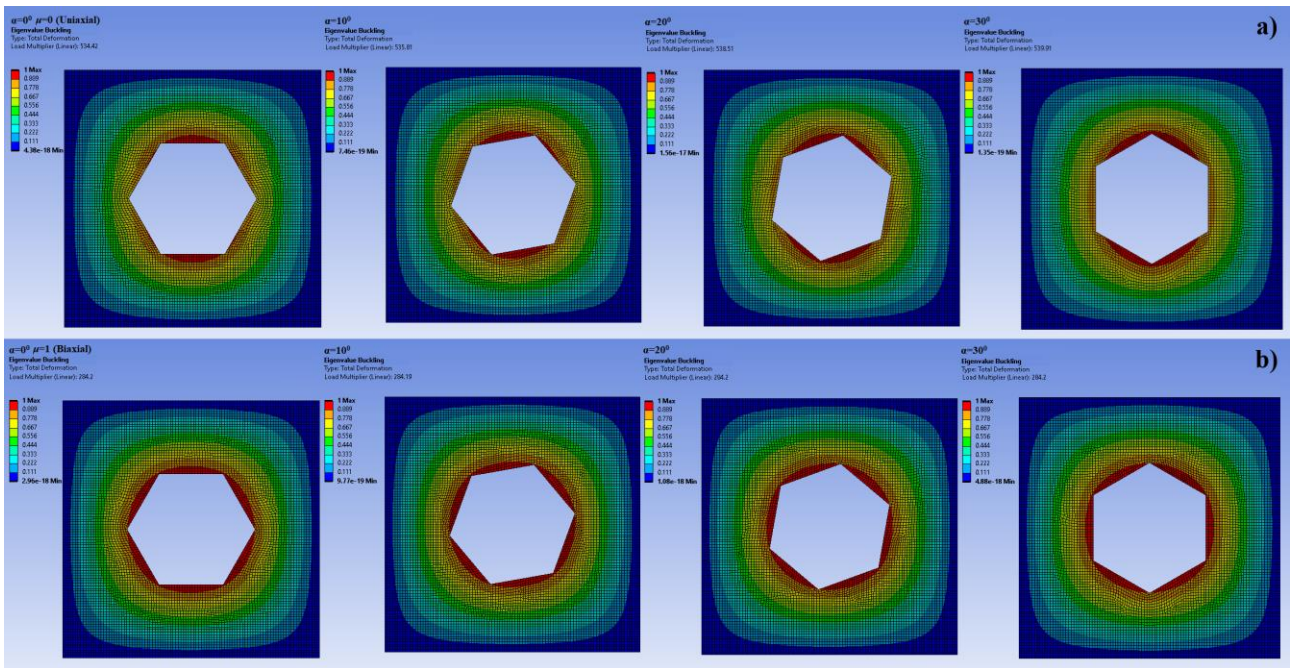


**Figure 10.** Contour plots of total deformations for hexagonal perforated plates with (a) uniaxial and (b) biaxial loading types ( $a/h=100$ )

Results of these performed buckling analyses also show the distribution of the total deformations in the hexagonal perforated square thin plate obtained as a result of the buckling mode analysis. Generally, the maximum deformation should be seen in the regions surrounding the hexagonal holes. The critical buckling loads calculated in the case of biaxial loadings are approximately half of those calculated in the case of uniaxial loadings. In hexagonal perforated plates under uniaxial loading, the regions with the highest total deformations are the hole edges parallel to the  $x=0$  and  $x=a$  edges, where the axial load is not loaded. On the other hand, in hexagonal perforated plates under biaxial loading, it is seen that the highest total deformation regions are distributed to all sides of the hole.

The contour plots of total deformations of four of ten different square perforated plates are given in Figure 11 as an example.

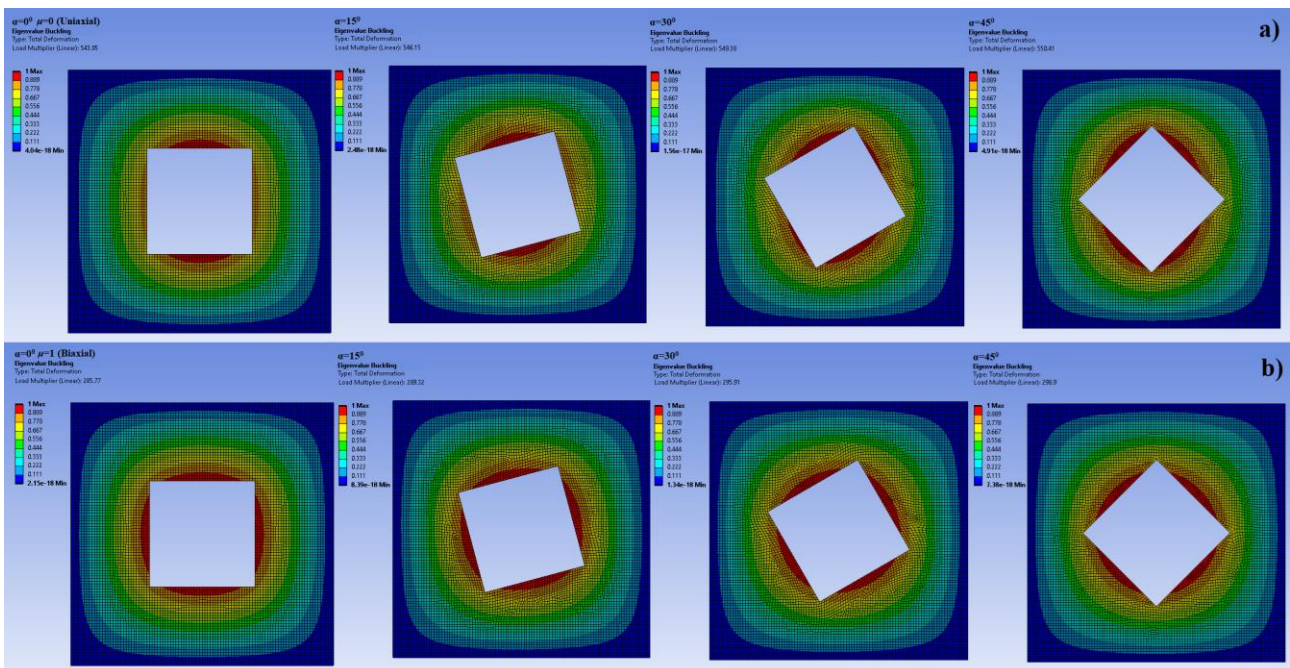


**Figure 11.** Contour plots of total deformations for square perforated plates with (a) uniaxial and (b) biaxial loading types ( $a/h=100$ )

Similar to perforated plates with hexagonal holes in perforated plates with square holes the maximum deformation should be seen generally in the regions surrounding the holes. The critical buckling loads of square perforated plates under bi axial loadings are approximately half of the plates under uniaxial loadings. In square perforated plates under uniaxial loading, the regions with the highest total deformations are the hole edges parallel to the  $x=0$  and  $x=a$  edges, where the axial load is not loaded. On the other hand, in square perforated plates under biaxial loading, it is seen that the highest total deformation regions are distributed to all sides of the hole.

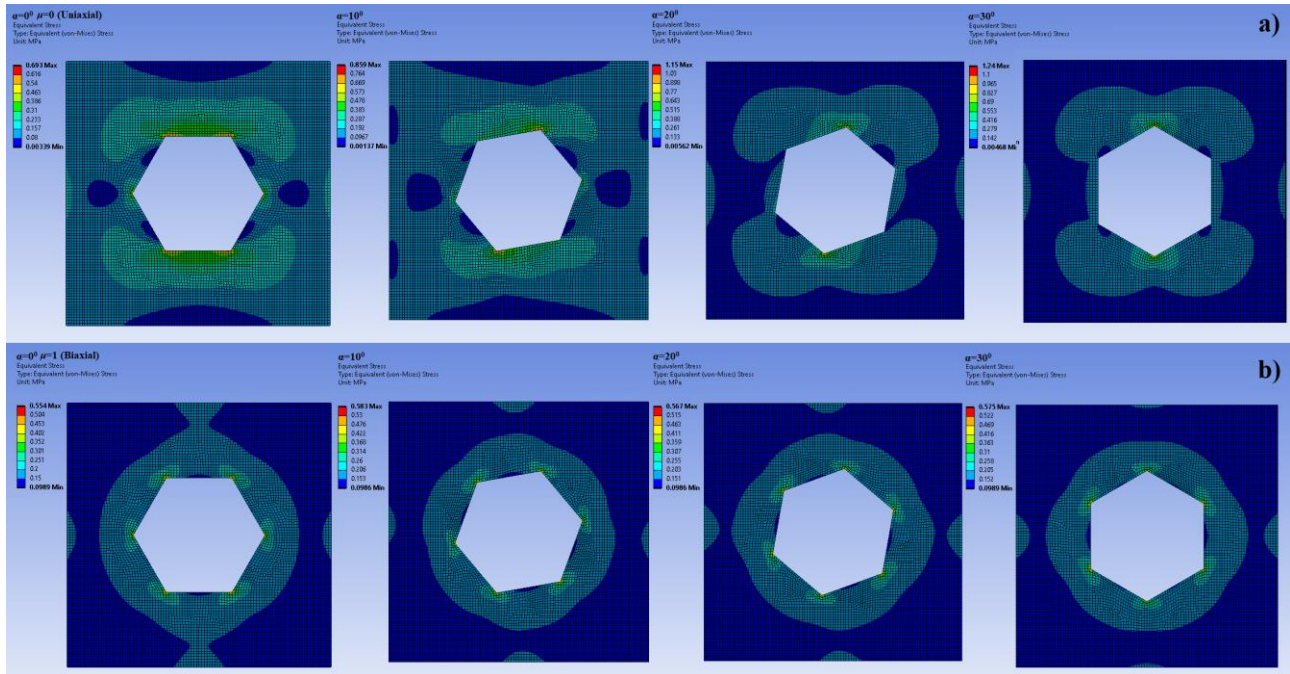


**Figure 12.** Von Mises stress of (a) uniaxial and (b) biaxial loaded hexagonal perforated plates with slenderness ratio of  $a/h=100$

The contour plots for Von Mises stress of four models of hexagonal perforated plates with orientation angles 0, 10, 20, and 30 degrees are given in Figure 12.

In uniaxial loaded hexagonal perforated plates stresses were condensed in surrounding the hole edges parallel to  $x$  axes. In biaxial loaded hexagonal perforated plates stresses were distributed all around the hole edges.

The contour plots for Von Mises stress of four models of square perforated plates with orientation angles 0, 10, 20, and 30 degrees are given in Figure 13.

In uniaxial loaded square perforated plates stresses were condensed in surrounding the hole edges parallel to  $x$  axes. In biaxial loaded square perforated plates, especially at the corners of the square hole stresses were distributed all around the hole edges.

## 5. Conclusion

In this study, the buckling behavior of simply supported perforated plates with different hole orientation angles was investigated. For determining the critical buckling loads different types of loads as uniaxial and biaxial in-plane compressive loads are affected. Square plates subjected to in-plane compressive load  $N_x$  in the edges of the square plate parallel to  $y$  axis were examined as uniaxial loading. For investigating the biaxial buckling loads of perforated simply supported square plates, in addition to the  $N_x$  load acting on the plate sides parallel to the  $y$  axis, a load equal to  $\mu$  times the  $N_x$  load was applied to the sides parallel to the  $x$  axis. The constant  $\mu$ , which shows how many times the buckling load  $N_x$  load acting on the plate edges parallel to the  $x$  axis was considered as 0, 0.5, 1 and 2.

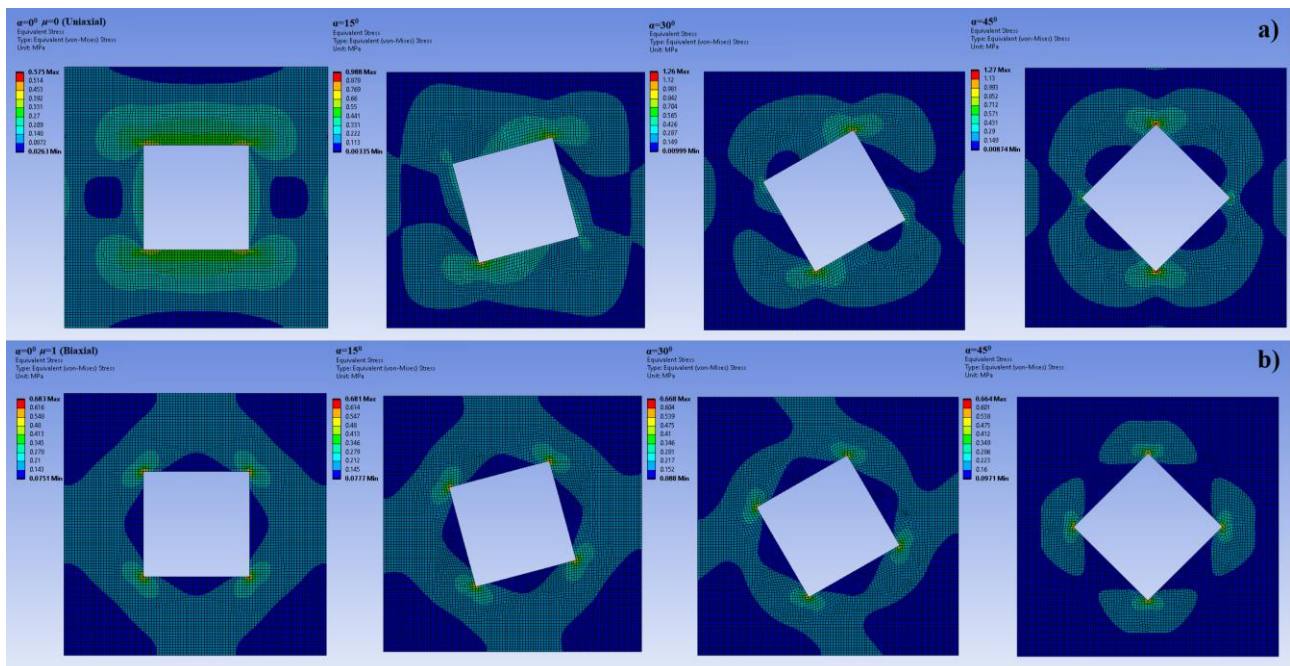


**Figure 13.** Von Mises stress of (a) uniaxial and (b) biaxial loaded square perforated plates with slenderness ratio of  $a/h=100$

The slenderness ratio is a parameter on buckling of perforated simply supported square plates. Three different slenderness ratios are considered in examples as 10, 50, and 100. The results obtained about the slenderness ratio can be summarized as follows:

- When the slenderness ratio decreases the critical buckling loads were increases.
- It is observed from the results that the slenderness ratio does not affect the corresponding increase of critical buckling load with the increase of hole orientation.
- As the slenderness ratio decreases, the critical buckling loads for the same orientation angles converge.
- The change in slenderness ratio affects the critical buckling load sequence obtained for hole types.

Perforated plates in the study have one hole in the middle of the plate. Centrally located hole perforation shapes are considered circular, hexagonal, and square. All the hole areas are taken as equal. The hexagonal hole was taken as a reference and the other hole areas were calculated based on the area of the hexagonal hole. The edge length of the hexagonal hole is quarter ( $1/4$ ) of the square plate edge length. It has been determined from the analyses that the effect of the hole types on critical buckling load is different for uniaxial and biaxial loading.

In uniaxial loadings, the results obtained about the hole types can be summarized as follows:

- For uniaxial loading, behave of the function of critical buckling load versus orientation angle of the perforation is quadratic function for square type perforations, sinusoidal function of two periods for hexagon type perforations, and constant linear function for circle type perforations.
- For the circle type perforations, critical buckling loads are the minimum values for  $a/h=100$  compared to hexagon and square. When the slenderness ratio  $a/h$  decreases to 20, the critical buckling load values are also lower than the square but higher than the hexagon type between some orientations. For the slenderness ratio  $a/h=10$ , the values are higher than the square and hexagonal type perforations for certain values of the orientation angle.
- For the hexagonal type perforations, critical buckling load values are generally seen as higher than the circle type perforations but lower than the square type perforations.
- For the square type perforations, critical buckling load values are mostly higher than the circle and hexagonal type perforations.

In biaxial loadings, the results obtained about the hole types can be summarized as follows:

- For biaxial loading, behave of the function of critical buckling load versus orientation angle of the perforation is quadratic function for square type perforations and constant linear function for hexagon and circle type perforations.

- For the circle type perforations, critical buckling loads are the minimum values for  $a/h=100$  and  $a/h=20$  compared to hexagon and square. When the slenderness ratio  $a/h$  decreases to 10, the critical buckling load values are higher than square type perforation at between 0 to 10 and 80 to 90 degrees of orientation angle.
- The critical buckling load in hexagon type holes is always higher than in circle type holes at all the slenderness ratios examined. However, hexagon type holes are higher than the square type holes only at between 0 to 10 and 80 to 90 degrees of orientation angle.
- For the square type perforations, critical buckling load values are mostly higher than the circle and hexagonal type perforations, as is the case with uniaxial loadings.

As a result of rotating the hole geometry in the perforated plate with the  $x$ - $y$  plane by an orientation angle  $\alpha$  around the  $z$  axis passing through its center, it was observed that the calculated critical buckling load did not remain the same although the hole areas were the same.

### Author contribution

For this study, the author responsible for the investigation, conceptualization, the development of the methodology, writing-original draft preparation, software data curation, validation, visualization is Mustafa Halûk Saraçoğlu; the author responsible for the investigation, conceptualization, the development of the methodology, writing, formal analysis, software data curation, software, validation, visualization is Fethullah Uslu; the author responsible for the investigation, methodology, the development of the methodology, writing-reviewing and editing, supervision is Uğur Albayrak.

### Declaration of ethical code

The authors of this article declare that the materials and methods used in this study do not require ethical committee approval and/or legal-specific permission.

### Conflicts of interest

The authors declare that there is no conflict of interest.

### References

- Al Qablan, H. (2022). Applicable formulas for shear and thermal buckling of perforated rectangular panels. *Advances in Civil Engineering*, 2022, <https://doi.org/10.1155/2022/3790462>
- Al Qablan, H., Rabab'ah, S., Abu Alfoul, B., & Al Hattamleh, O. (2022). Semi-empirical buckling analysis of perforated composite panel. *Mechanics Based Design of Structures and Machines*, 50(8), 2635-2652 <https://doi.org/10.1080/15397734.2020.1784198>
- Albayrak, U., & Saraçoğlu, M. H. (2018). Analysis of regular perforated metal ceiling tiles. *International Journal of Engineering and Technology*, 10(6), 440–446. <https://doi.org/10.7763/ijet.2018.v10.1099>
- Baumgardt, G. R., Fragassa, C., Rocha, L. A. O., dos Santos, E. D., da Silveira, T., & Isoldi, L. A. (2023). Computational model verification and validation of elastoplastic buckling due to combined loads of thin plates. *Metals*, 13(4), 731–751. <https://doi.org/10.3390/MET13040731>
- Brown, C. J., Yettram, A. L., & Burnett, M. (1987). Stability of plates with rectangular holes. *Journal of Structural Engineering*, 113(5), 1111–1116. [https://doi.org/10.1061/\(ASCE\)0733-9445\(1987\)113:5\(1111\)](https://doi.org/10.1061/(ASCE)0733-9445(1987)113:5(1111))
- Bryan, G. H. (1891). *On the stability of a plane plate under thrusts in its own plane with applications to the buckling of the sides of a ship. Proceedings of London Mathematics Society*, s1-22(1), 54–67. <https://doi.org/10.1112/plms/s1-22.1.54>
- Chow, F.-Y., & Narayanan, R. (1984). *Buckling of plates containing openings. 7th International Specialty Conference on Cold-Formed Steel Structures*, 39–53. <https://scholarsmine.mst.edu/isccss/7iccfss/7iccfss-session2/1>

- Dehadray, P.M., Alampally, S., & Lokavarapu, B. R. (2021). *Buckling analysis of thin isotropic square plate with rectangular cut-out*. *International Conference on Innovations in Mechanical Engineering*, 71–86. [https://doi.org/10.1007/978-981-16-7282-8\\_6](https://doi.org/10.1007/978-981-16-7282-8_6)
- Fu, W. & Wang, B. (2022). A semi-analytical model on the critical buckling load of perforated plates with opposite free edges. *Original Research Article Proc IMechE Part C: J Mechanical Engineering Science*, 236(9), 4885–4894. <https://doi.org/10.1177/09544062211056890>
- Guo, Y. & Yao, X. (2021). Buckling behavior and effective width design method for thin plates with holes under stress gradient. *Mathematical Problems in Engineering*, 2021. <https://doi.org/10.1155/2021/5550749>
- Jayabalan, J., Dominic, M., Ebid, A. M., Soleymani, A., Onyelowe, K. C., & Jahangir, H. (2022). Estimating the buckling load of steel plates with center cut-outs by ANN, GEP and EPR techniques. *Designs*, 6(5), 84-96. <https://doi.org/10.3390/DESIGNS6050084>
- Karakaya, C. (2022). Numerical investigation on perforated sheet metals under tension loading. *Open Chemistry*, 20(1), 244–253. <https://doi.org/10.1515/chem-2022-0142>
- Kharchenko, S., Kharchenko, F., Samborski, S., Paśnik, J., Kovalyshyn, S., & Sirovitskiy, K. (2022). Influence of physical and constructive parameters on durability of sieves of grain cleaning machines. *Advances in Science and Technology Research Journal*, 16(6), 156–165. <https://doi.org/10.12913/22998624/156128>
- Saraçoğlu, M. H., Uslu, F., & Albayrak, U. (2021). Investigation of hole shape effect on static analysis of perforated plates with staggered holes. *International Journal of Engineering and Innovative Research*, 3. <https://doi.org/10.47933/ijeir.883510>
- Silveira, T., Neufeld, J. P. S., Rocha, L. A. O., Santos, E. D., & Isoldi, L. A. (2021). *Numerical analysis of biaxial elasto-plastic buckling of perforated rectangular steel plates applying the Constructal Design method*. *IOP Conference Series: Materials Science and Engineering*, 1048(1), 012017. <https://doi.org/10.1088/1757-899X/1048/1/012017>
- Swanson Analysis System Inc., A. (2005). *ANSYS User's manual*.
- Timoshenko, S., & Woinowsky-Krieger, S. (1959). *Theory of plates and shells*. In McGraw-Hill, Inc. McGraw-Hill, Inc.
- Uslu, F., Saraçoğlu, M. H., & Albayrak, U. (2022). Buckling of square and circular perforated square plates under uniaxial loading. *Journal of Innovations in Civil Engineering and Technology*, 4(2), 61–75. <https://dergipark.org.tr/en/pub/jiciviltech/issue/74932/1190956>